Crystals **2012**, *2*, 984-995; doi:10.3390/cryst2030984

OPEN ACCESS

crystals

ISSN 2073-4352

www.mdpi.com/journal/crystals

Review

Paramagnetic Metal—Antiferromagnetic Insulator Transition in *π-d* System λ-$BETS_2FeCl_4$, BETS = Bis(ethylenedithio)tetraselenafulvalene

Hiroshi Akiba *, Kazuo Shimada, Naoya Tajima, Koji Kajita and Yutaka Nishio

Department of Physics, Faculty of Science, Toho University, Funabashi, Chiba 274-8510, Japan; E-Mails: 6411011s@nc.toho-u.ac.jp (K.S.); naoya.tajima@sci.toho-u.ac.jp (N.T.); kajita@ph.sci.toho-u.ac.jp (K.K.); nishio@ph.sci.toho-u.ac.jp (Y.N.)

***** Author to whom correspondence should be addressed; E-Mail: h-akiba@issp.u-tokyo.ac.jp; Tel.: +81-47-472-6991; Fax: +81-47-472-6988.

Received: 23 April 2012; in revised form: 1 July 2012 / Accepted: 2 July 2012 / Published: 17 July 2012

Abstract: Quasi-two-dimensional organic conductor λ-$BETS_2FeCl_4$ (BETS = bis(ethylenedithio)tetraselenafulvalene) transforms from a paramagnetic metal (PM) to an antiferromagnetic insulator (AFI) at a transition temperature, T_{MI}, of 8.3 K under zero magnetic field. To understand the mechanism of this PM-AFI phase transition, we studied the thermodynamic properties of λ-$BETS_2FeCl_4$. We observed, below T_{MI}, a six-level Schottky hump in its specific heat and a broad shoulder in its magnetic susceptibility. Just below the transition temperature T_{MI}, about 80% of 3*d* spin degree of freedom is sustained. These temperature dependences clarify that π and 3*d* spins do not cooperatively form the AF order at T_{MI}. In λ-$BETS_2Fe_xGa_{1-x}Cl_4$ system, the increasing Fe 3*d* spin density enhances the internal magnetic field caused by π spin antiferromagnetic (AF) ordering, although the 3*d* spin itself maintains large entropy against the AF ordering. It was confirmed that the Fe 3*d* spin provided favorable conditions for this mysterious PM-AFI phase transition in the π electron system. We propose that this phase transition originates from the magnetic anisotropy introduced by the *π-d* interaction, which suppressed the low dimensional fluctuation in the π spin system.

Keywords: organic conductor; *π-d* interaction; PM-AFI phase transition; specific heat; magnetic susceptibility

---

1. Introduction

Several researchers have studied λ and κ-type organic conductors to discuss the relationship between magnetic ordering and superconductivity [1–3]. The quasi-two-dimensional organic superconductor λ-$BETS_2FeCl_4$ has a layered structure in which conductive layers composed of BETS molecules, and insulating layers composed of $FeCl_4$ molecules with high-spin state of Fe (s_d = 5/2) are arranged alternately [1]. It exhibits the magnetic field-induced superconductivity above 17 T [4], and a novel metal-insulator (MI) transition accompanied by antiferromagnetic (AF) ordering at T_{MI} = 8.3 K under zero magnetic field [5,6]. In contrast, the isostructural nonmagnetic conductor λ-$BETS_2GaCl_4$ does not exhibit an MI transition, although it does exhibit a superconducting (SC) transition [7,8]. In the λ-$BETS_2Fe_xGa_{1-x}Cl_4$ alloys, the PM-AFI transition is suppressed as x decreases, and then the ground state changes to a SC phase for $x \leq 0.35$ from the AFI phase. It is remarkable that two successive phase transitions PM-SC-AFI take place for $0.35 \leq x \leq 0.5$ with decreasing temperature [9]. These facts led researchers to believe that the notable magnetic and electronic properties of λ-$BETS_2FeCl_4$ were derived from the magnetic Fe ions present in the salt. In the earlier studies, it was concluded that the Fe 3*d* spin dominantly contributed to the formation of AF ordering, thus bringing AF ordering as well as MI transition to the π electron system [1].

In these materials, Negishi *et al.* reported thermal anomaly below T_{MI} [10]. However, its origin is still unknown. In order to thermodynamically investigate how the AF ordering, which was thought to be a combination of 3*d* spin and π spin, is formed, we measured the specific heats of λ-$BETS_2MCl_4$ (M = Fe, Ga) and these mixed crystal systems down to 0.2 K.

We measured the specific heat by the thermal relaxation method. The sample holder made of the Stycast 1266 was located in the mixing chamber of a dilution refrigerator. A vacuum inside the holder was produced using charcoal. Since heat-contact of a thermal bath with a ^{3}He-^{4}He mixture in the mixing chamber was suppressed, the specific heat measurement in a wide temperature range from 0.2 to 12 K could be possible. We attached several single crystals (total sample weight: 0.120 mg) to a bolometer with Apiezon N grease. The magnetic susceptibility measurements were carried out under an external magnetic field H of 0.1 T with a superconducting quantum interference device (SQUID) magnetometer (Magnetic Property Measurement System). The evaluations of Fe contents in a mixed crystal λ-$BETS_2Fe_xGa_{1-x}Cl_4$ were carried out using electron probe microanalysis (EPMA).

2. Results and Discussion

*2.1. Large 3*d *Spin Degrees of Freedom*

We measured the specific heat of λ-$BETS_2FeCl_4$ and nonmagnetic λ-$BETS_2GaCl_4$ by the thermal relaxation method. The specific heat of $FeCl_4$ and $GaCl_4$ salts are indicated by open and closed circles in Figure 1, respectively. The specific heat of $FeCl_4$ salt shows a sharp peak at the MI transition temperature (T_{MI} ~ 8.3 K) and has a larger value than that of $GaCl_4$ salt at the entire temperature region. In order to study the excess components of the $FeCl_4$ salt in detail, we first estimated its lattice and electronic specific heat. We assumed that the specific heat of isostructural $GaCl_4$ salt was equivalent to the lattice specific heat of $FeCl_4$ salt.

Figure 1. Temperature dependencies of the specific heat of λ-$BETS_2FeCl_4$ (○) and λ-$BETS_2GaCl_4$ (●). Reproduced with permission from JPSJ [11].

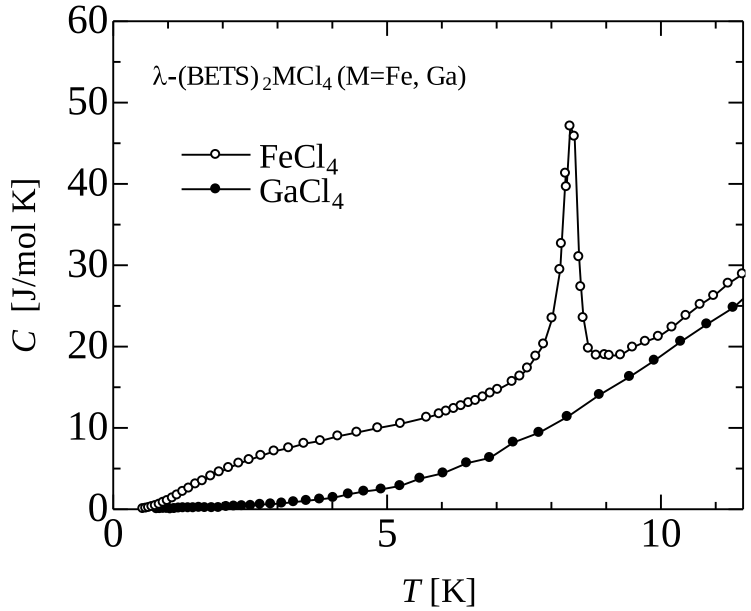

The electronic specific heats of these two salts were clearly different since the $GaCl_4$ salt exhibited superconductivity at 5.5 K, while the $FeCl_4$ salt underwent an MI transition at 8.3 K. Around 5.5 K, the $GaCl_4$ salt exhibited superconductivity of the BCS type and showed the specific heat jump 1.43 γT J/mol K [12]. Considering the difference in these electronic specific heats, we obtained the excess specific heats ΔC (shown in Figure 2) by subtracting the lattice and electronic specific heats in the PM phase, and subtracting the lattice contribution in the AFI phase, respectively.

Figure 2. Excess specific heat ΔC of λ-$BETS_2FeCl_4$ by subtracting the lattice and the electric specific heat estimated for λ-$BETS_2GaCl_4$. The solid curve shows the calculated specific heat based on the paramagnetic 3d spin (Fe^{3+} s_d = 5/2) system under the internal magnetic field $H_{\pi d}$ = 4.0 T. The inset shows the energy levels of s_d = 5/2 caused by Zeeman splitting. Reproduced with permission from JPSJ [11].

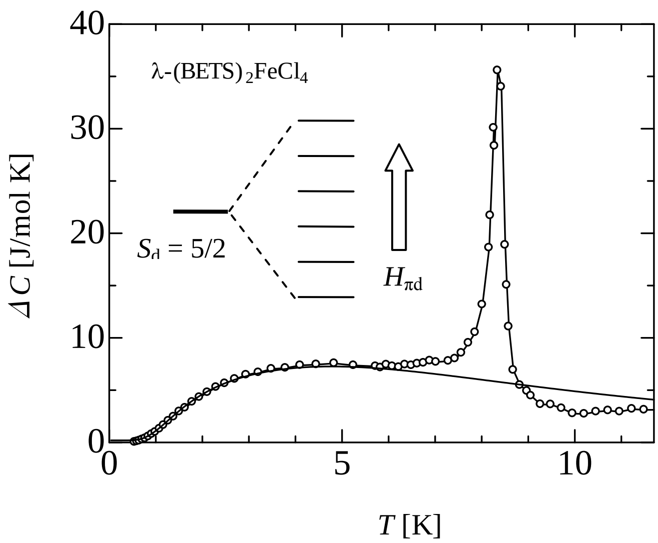

The open circles in Figure 2 show the excess specific heat Δ*C* obtained by subtraction of the lattice and electronic specific heat estimated for the $GaCl_4$ salt from the total specific heat of the $FeCl_4$ salt. A sharp peak was observed at 8.3 K. It should be noted that a broad hump that appears to be a Schottky-type anomaly was found in a lower temperature side of the sharp peak. If the π and 3*d* spins cooperatively align antiferromagnetically below T_{MI}, as was expected for the present system, the larger peak of the specific heat would only exist at T_{MI}, followed by a rapid reduction without the formation of the hump. This behavior is completely different from that of Δ*C* in Figure 2. We can speculate that the Schottky-type specific heat is derived from the paramagnetic 3*d* spin under the internal magnetic field induced by the π-*d* interaction.

Since the Schottky-type anomaly occurs for 3*d* or π spin systems only under the influence of a magnetic field, we calculated the temperature dependence of the specific heat of the 3*d* spin $s_d = 5/2$ and π spin $s_\pi = 1/2$ systems for paramagnetic states and obtained the best fit for the excess specific heat Δ*C* in the case of the Fe^{3+} 3*d* spin. The energies at $s_d = 5/2$ were split into six levels by the Zeeman splitting under an internal magnetic field $H_{\pi d}$ ascribed to the π-*d* interactions, as shown in the inset of Figure 2. On the basis of the results of the energy splitting, we estimated the internal magnetic field $H_{\pi d}$ from the π spin to the 3*d* spin as 4.0 T, while the internal magnetic field $H_{d\pi}$ caused by the 3*d* spin to the π electron was estimated as $H_{d\pi}$ = 33 T from the experimental results of the field-induced superconductivity [4,13]. We consider that this disagreement is mainly due to the different origins (s_π and s_d) of $H_{\pi d}$ and $H_{d\pi}$.

The integration of Δ*C*/*T* was performed to estimate the entropy *S*, which derives information about the degrees of freedom, as shown in Figure 3. The resulting entropy was close to a value of *R*ln6 (*R*ln6 = 14.9 J/mol K), *i.e.*, the spin degrees of freedom for the 3*d* spin (*R*ln($2s_d + 1$), $s_d = 5/2$). These experimental results suggest that the 3*d* spin degrees of freedom give a large contribution to the sharp peak as well as the Schottky-type hump. It should be noted that about 80% of the 3*d* spin degrees of freedom is sustained just below T_{MI}.

Figure 3. Temperature dependencies of spin entropy of λ-$BETS_2FeCl_4$ calculated from Δ*C* (○), calculated from specific heat of Schottky-type (solid curves). The dashed line shows the degrees of freedom for 3*d* spins. Reproduced with permission from JPSJ [11].

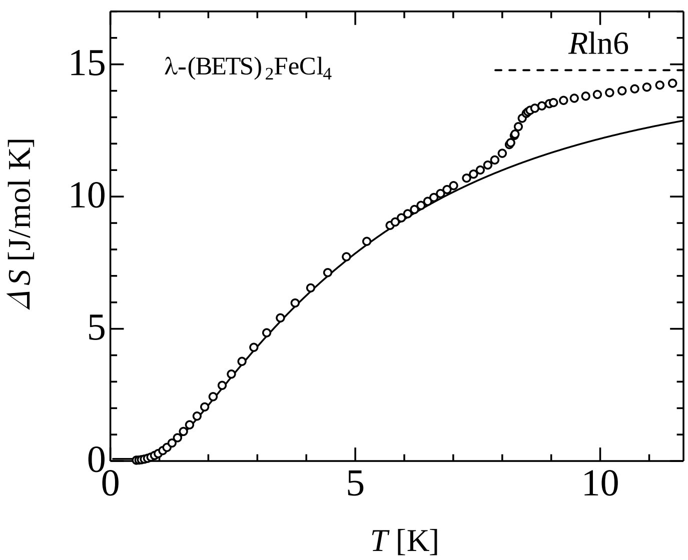

At MI transition, π electron system transfers from the Pauli paramagnetic metal state having the entropy of π electron $S_\pi = \gamma T$ to the antiferromagnetic insulator with $S_\pi = 0$ because of the strong π-π exchange interaction $J_{\pi\pi}/k_B$ = 448 K, which is much larger than the metal-insulator transition temperature T_{MI} [14]. The entropy difference ΔS_π in both phases corresponds to the $\gamma T_{MI} = 0.014 \times 8.3 = 0.17$ J/mol K by assuming that the electronic density of the states at Fermi level is the same with that of $GaCl_4$ salt [12]. Its value is much smaller than the observed 3*d* contribution *R*ln6. From this result of entropy, we could not detect the large reductions of *R*ln2 ~ 5.7 J/mol K accompanied with the AF ordering of π spin ($s_\pi = 1/2$). Combining the metal-insulator transition is a remarkable feature of this novel AF spin alignment.

2.2. Magnetic and Thermal Properties in AFI Phase

The magnetic susceptibility provides information about the direction and magnitude of the internal magnetic field $H_{\pi d}$. To clarify the origin of the splitting of the 3*d* spin state, we examined the magnetic susceptibility. Figure 4 illustrates the magnetic susceptibility observed under application of an external field *H* of 0.1 T along the *c*-axis. Above T_{MI}, the magnetic susceptibility *M*/*H* shows Curie-Weiss-type behavior for $s_d = 5/2$. At T_{MI}, it shows a sharp step down, and subsequently, *M*/*H* reduces with decreasing temperature. We also find that *M*/*H* has a shoulder-shaped anomaly below T_{MI}. This characteristic shoulder is observed in the curve at low temperatures, corresponding to the region where the Schottky-type specific heat anomaly is also observed. These findings suggest a common origin of the shoulder in the magnetic susceptibility curve and the Schottky-type specific heat.

Figure 4. Magnetic susceptibility *M*/*H* of λ-$BETS_2FeCl_4$ under an external magnetic field parallel to the *c*-axis. The solid and dashed curves show the magnetic susceptibility calculated on the basis of the paramagnetic 3*d* spin model and Curie–Weiss law, respectively. Reproduced with permission from JPSJ [15].

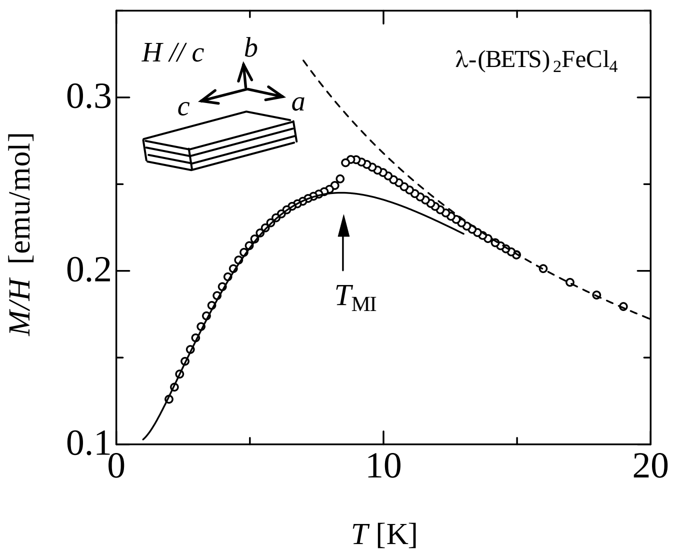

This internal magnetic field $H_{\pi d}$ is generated by the exchange interaction $J_{\pi d}$ with the AF-ordered π spin system. The π-*d* interaction having the shortest contact was found to be the strongest coupling between several π-*d* couplings [14]. Assuming that this coupling dominates the internal magnetic field

$H_{\pi d}$, we may ignore the other weak couplings and propose a possible spin structure in the AFI phase, as shown in Figure 5a. In this case, the internal magnetic field on the 3*d* spin induced by the nearest neighbor π spin is alternately oriented in the opposite direction. Since the alternating internal magnetic field begins to align the 3*d* spins as the temperature decreases, the magnetization of the 3*d* spin system will be canceled out, and so will gradually decrease in the AFI phase.

Figure 5. (**a**) Schematic view of the π and 3*d* spin structure in the AFI phase. The open and closed arrows represent π spin $s_\pi = 1/2$ localized at the BETS dimer and Fe 3*d* spin $s_d = 5/2$, respectively. After the AF ordering of π spin, the internal fields $+H_{\pi d}$ and $-H_{\pi d}$ are expected at the Fe sites. (**b**) Effective magnetic field H_{eff}^+ (H_{eff}^-) at the Fe A (B) site with the external field H parallel to the *c*-axis and the internal field $+H_{\pi d}$ ($-H_{\pi d}$). The AF easy axis is confined to the *b***c* plane and makes an angle θ with respect to the *c*-axis [16].

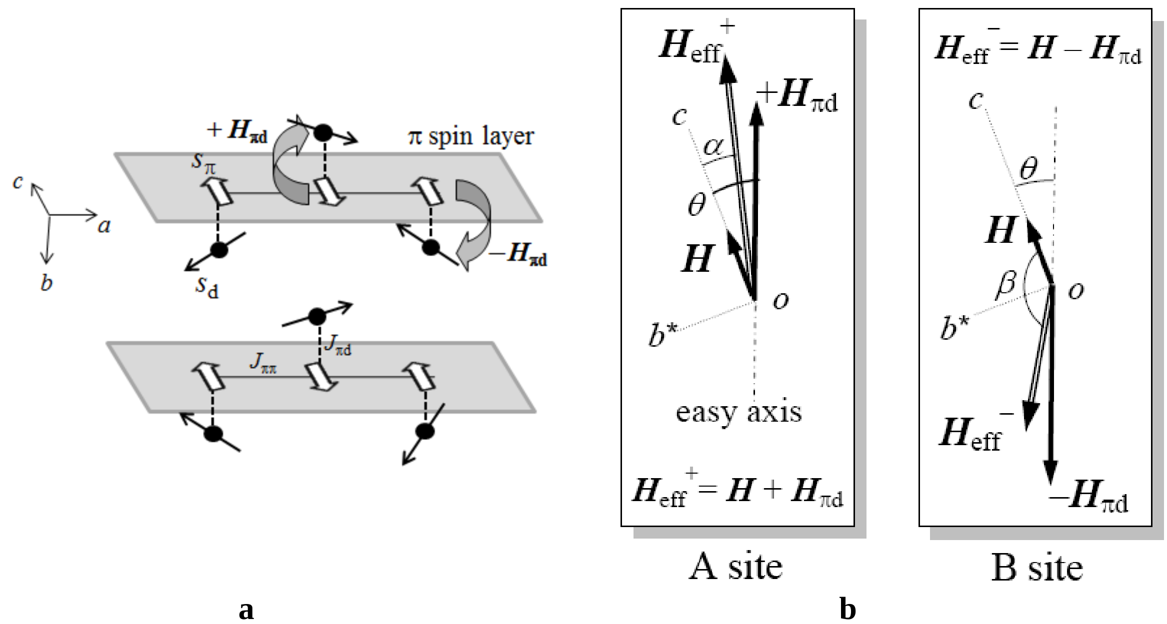

Next, we tried to reproduce the characteristic shoulder in the magnetic susceptibility on the basis of this spin model. Under the weak external field H = 0.1 T (<< spin-flop field H_{SF} ~ 1 T [6]), the π spin system forms AF alignment along the easy axis and produces the internal magnetic fields $+H_{\pi d}$ and $-H_{\pi d}$ on the Fe 3*d* spin at sites A and B, respectively, where the effective magnetic field $H_{eff}^{\pm}$ becomes $H_{eff}^{\pm} = H \pm H_{\pi d}$, as shown in Figure 5b. We calculated the magnetizations M_d^+ and M_d^- at sites A and B, respectively, using the Brillouin function $B_s(x)$ as

$$M_d^{\pm} = \frac{N}{2} g\mu_B s_d B_s \left[\frac{g\mu s_d H_{eff}^{\pm}}{k_B T}\right] \tag{1}$$

In this study, the external magnetic field is applied along the *c*-axis. According to the torque measurement by Sasaki *et al.* [16], the *c*-axis is tilted by about θ = 30° from the easy axis. Considering the tilt angle θ, the total magnetization component M_d parallel to H can be obtained as

$$M_d = M_d^+ \cos(\alpha) + M_d^- \cos(\beta) \tag{2}$$

where the angles α between H and H_{eff}^{+} and β between H and H_{eff}^{-} can be determined from θ, $H_{\pi d}$, and H (see Figure 6b). The calculated magnetic susceptibility M_d/H can well reproduce the resulting data, as shown by the solid curve in Figure 4, using the following parameter values: H = 0.1 T, θ = 25°, and $H_{\pi d}$ = 4 T. The strength of this internal field is in good agreement with the value estimated from the Schottky specific heat. In addition, Waerenborgh *et al.* observed sextet Fe Mössbauer signals generated by an internal magnetic field $H_{\pi d}$, which supports the paramagnetic model of the Fe 3*d* spin [17].

Figure 6. (**a**) Temperature dependence of specific heat for mixed crystals λ-$BETS_2Fe_xGa_{1-x}Cl_4$ (○) and λ-$BETS_2$GaCl4 (●). (**b**) Excess specific heat ΔC of λ-$BETS_2$FexGa$_{1-x}Cl_4$ obtained by subtracting lattice and electric specific heats estimated for λ-$BETS_2GaCl_4$.

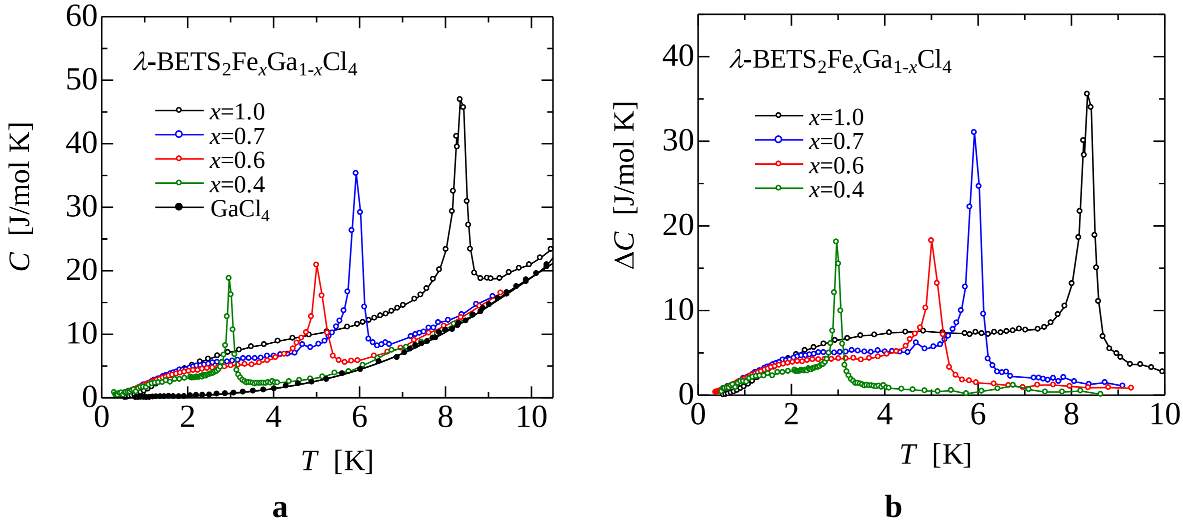

In the high-temperature metallic phase, the magnetic susceptibility follows the Curie-Weiss law with 3*d* spin s_d = 5/2, as shown by the dashed curve in Figure 4. It is notable that over the entire temperature range studied, the Fe 3*d* spin paramagnetic states dominate the magnetic susceptibility and specific heat. Because we can expect that for the π spin system, the temperature-independent Pauli paramagnetic susceptibility χ_{Pauli} is approximately 3 × 10^{-4} emu, which is three orders of magnitude smaller than that for Fe 3*d* predicted by the Curie-Weiss law, assuming that the electronic density of states at the Fermi level is the same as that for λ-$BETS_2GaCl_4$ [12].

At T_{MI}, the paramagnetic metal PM-AFI transition causes a sharp step down. In the metallic region, the interaction working on the 3*d* spins is of the Ruderman-Kittel-Kasuya-Yoshida (RKKY) type via the conduction π electrons [18]. Across the MI transition, this spin network will be cut off by the localization of π electrons. Therefore, the magnetic susceptibility curve of 3*d* spin changes from following the Curie-Weiss law (dashed curve in Figure 4) to the present paramagnetic model (solid curve in Figure 4). The 3*d* spin dominates the step down at T_{MI} and the slow reduction in the AFI phase.

2.3. Role of Fe 3d *Spin in PM-AFI Transition*

Figure 6a shows the specific heats of mixed crystals λ-$BETS_2Fe_xGa_{1-x}Cl_4$ (0.4 < x ≤ 1) and λ-$BETS_2GaCl_4$. The specific heats of λ-$BETS_2Fe_xGa_{1-x}Cl_4$ show sharp peaks at T_{MI} or SC-AFI transition temperature T_{SCI} and broad humps below these sharp peaks, while non-magnetic λ-$BETS_2GaCl_4$ does not exhibit these anomalies. Because the specific heat of λ-$BETS_2Fe_xGa_{1-x}Cl_4$ in the metallic phase was close to that of λ-$BETS_2GaCl_4$ in the metallic phase, we assumed that the lattice and electronic specific heats of isostructural λ-$BETS_2GaCl_4$ were equivalent to those of λ-$BETS_2Fe_xGa_{1-x}Cl_4$. We obtained the excess specific heats ΔC (shown in Figure 6b) by subtracting the estimated lattice and electronic specific heat in the metal phase, and subtracting the lattice contribution in the AFI phase, respectively. In Figure 6a, broad humps are found below sharp peaks for all mixed crystals. This large value for ΔC in the low-temperature AFI phase suggests that a majority of the spin degrees of freedom in this system were maintained even after transition to the AFI phase was achieved. These anomalies in the AFI ground state of the mixed crystals contrast the critical behavior that in *π-d* system κ-$BETS_2FeBr_4$, Fe 3*d* spin (s_d = 5/2) takes place at AF transition at Neel temperature [19,20].

Figure 7 shows the excess entropies obtained by integrating $\Delta C/T$ over temperature. The resulting total entropies were close to the values of xR ln6 (dashed line in Figure 7) expected for the degrees of freedom of 3*d* high spins (s_d = 5/2) per molecular formula. These experimental results suggest that the 3*d* spin degrees of freedom contributed substantially to the sharp peaks as well as the Schottky-type humps for all mixed crystals. During transition, *π* spin resulted in AF ordering and produced a strong internal magnetic field at the nearest neighboring Fe sites. At the transition temperature, an increase in the intensity of the internal magnetic field at the Fe sites caused a rapid reduction in 3*d* spin entropy, indicated by sharp peaks in the specific heats.

Figure 7. Temperature dependencies of spin entropy of λ-$BETS_2Fe_xGa_{1-x}Cl_4$ calculated from ΔC. The dashed lines show the degrees of freedom for 3*d* spins for values of xRln6.

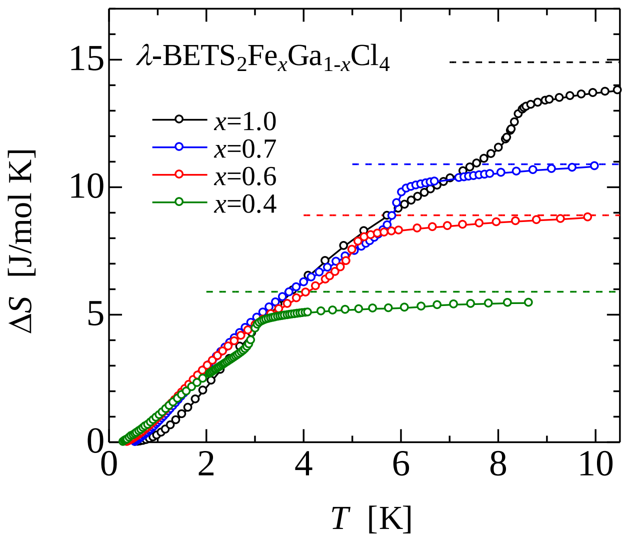

To discuss the origin of this transition, we investigated the dependence of excess specific heat on Fe content. Figure 8a indicates excess specific heats normalized by Fe content $\Delta C/x$. The maximum of these broad humps gradually shifts to a lower temperature with decreasing *x*. The broad humps of all mixed crystals could be fitted to the calculated Schottky specific heats of s_d = 5/2 (solid curves in Figure 8a).

Figure 8. (**a**) Temperature dependencies of excess specific heat divided by Fe content $\Delta C/x$. The solid curves show the 6-level Schottky specific heats, which are based on the paramagnetic 3*d* spin (s = 5/2) system under the internal magnetic field $H_{\pi d}$. The broad maximum of the Schottky specific heat shifts to lower temperature with decreasing $H_{\pi d}$. (**b**) Fe density dependence of $H_{\pi d}$.

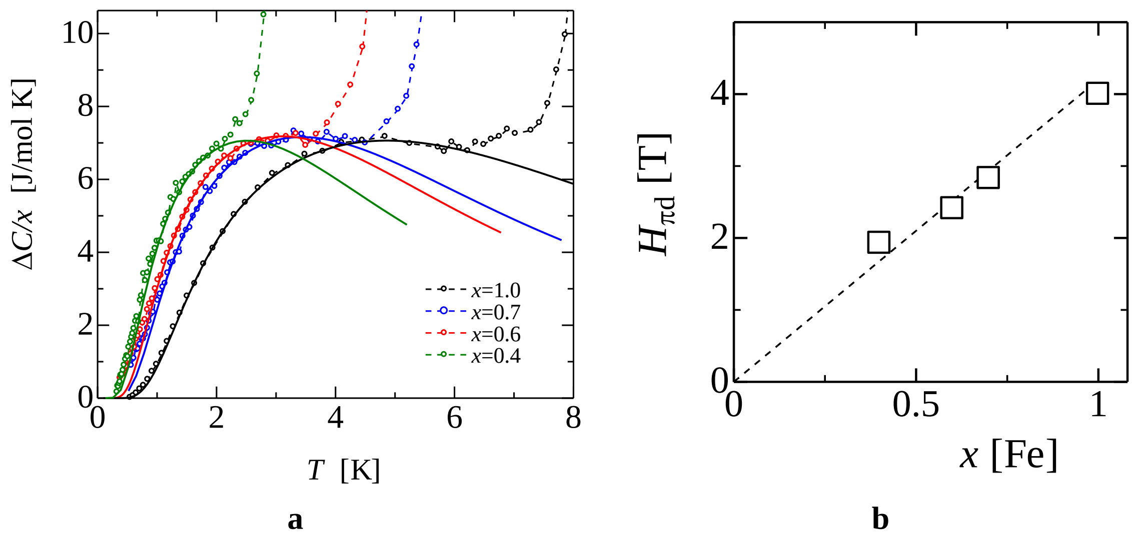

As we approach the transition temperature, the experimental data deviate from the solid curves because of the formation of sharp peaks. The sharp peaks are attributed to the rapid enhancement of the internal magnetic field at the Fe sites accompanied with the development of spontaneous magnetization in the π spin system. When the π magnetization reaches saturation, ΔC follows the calculated Schottky curves under fixed internal magnetic fields $H_{\pi d}$. The intensity of $H_{\pi d}$ estimated from the agreement between the ΔC data and the calculated curves were proportional to the x values, as shown in Figure 8b. However, these experimental results are very puzzling because the high density of *paramagnetic* Fe 3*d* spin increased the internal magnetic field $H_{\pi d}$, owing to the saturation magnetization of the AF ordered π spin and increased the PM-AFI transition temperature. These results clarify that the Fe 3*d* spin plays a crucial role in stabilizing AF ordering in the π spin system. Further analysis of the sharp peaks enables a measurement of the strong temperature dependence of the internal magnetic field in the vicinity of the transition temperature and gives information about a characteristic critical behavior of the spontaneous magnetization in the low-dimensional π spin system. The detailed studies of this critical behavior will be reported in our next paper.

Figure 9 shows a plot of $\Delta C/x$ *versus* the temperature normalized by each internal magnetic field $k_B T/g\mu_B H_{\pi d}$. These normalized data fit to one of the curves obtained at the temperatures studied. The sharp peaks as well as the Schottky-type broad humps could be normalized in the high Fe-content region of $x > 0.5$, where the PM-AFI transition occurs [9]. In the low Fe-content region ($0.3 < x < 0.5$), the Schottky term could be reduced to the same universal curve; however, the sharp peak at the phase transition could not be normalized, because at peak temperatures, the SC-AFI transition occurred instead of the PM-AFI transition (see the inset of Figure 9). It should be noted that at the PM-AFI transition, the phase transition temperatures as well as the Schottky specific heats could be scaled by internal magnetic field $H_{\pi d}$. These scaling rules clarify that the internal magnetic field drove the PM-AFI transition.

Figure 9. $\Delta C/x$ *versus* the temperature normalized by the internal magnetic field $k_B T/g\mu_B H_{\pi d}$. The inset is T-x phase diagram of λ-$BETS_2Fe_xGa_{1-x}Cl_4$ [9].

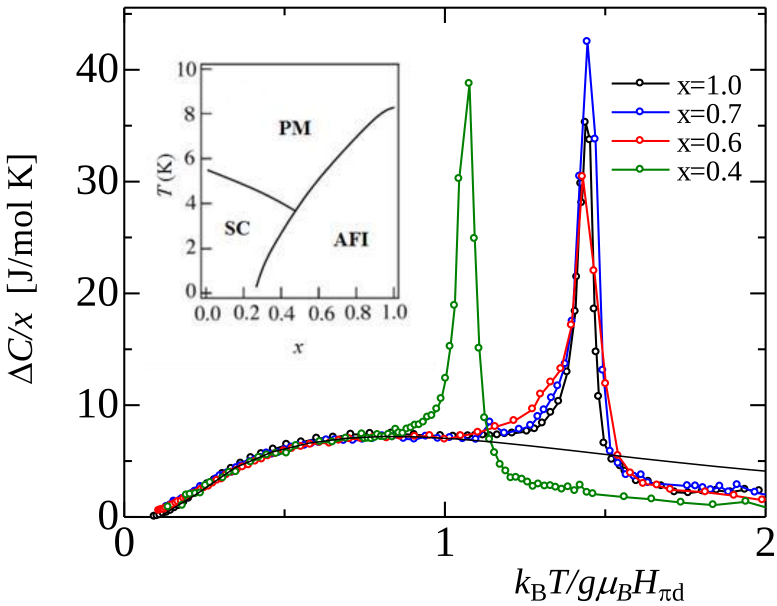

We have a possible explanation for the role of Fe 3*d* spins in PM-AFI transitions and propose a mechanism for this peculiar phase transition, in which the fluctuation of the π spin system is suppressed by magnetic anisotropy introduced by Fe 3*d* spin via the π-*d* interaction. Magnetic susceptibility measurements suggested that the π spin system, which exhibits isotropic magnetic properties in ordinary organic conductors, has finite anisotropy in λ-$BETS_2FeCl_4$ [5]. A decrease in Fe content weakens the anisotropic magnetic properties, *i.e.*, the spin-flop fields H_{SF} in magnetization [21]. These results suggest that the magnetic anisotropy of the π spin system originates from the anisotropic crystal field surrounding the Fe 3*d* spin system through the π-*d* interaction; this Fe-induced anisotropy suppresses two-dimensional fluctuation in the present π spin system and increases the PM-AFI transition temperature.

We have studied the critical behavior of the PM-AFI transition for the λ-$BETS_2FeCl_4$ system, measuring the excess magnetic specific heat. We estimated the critical process of the spontaneous magnetization of π spin in the vicinity of the transition temperature. We could observe the low dimensional criticality of the magnetization of π spin. We considered that the magnetic anisotropy induced by π-d interactions transfer the π spin from the two-dimensional (2D) Heisenberg spin system to the 2D Ising one having the easy axis. Antiferromagnetic order cannot be established in 2D Heisenberg spin systems. In contrast, 2D Ising spin system exhibits long-range magnetic order. To find unambiguous evidence for 2D long-range ordering in the AFI phase, a more detailed study on the criticality of this phase transition is now in progress.

3. Conclusions

We have studied the thermodynamic properties of λ-$BETS_2Fe_xGa_{1-x}Cl_4$ ($0 \leq x \leq 1$) to clarify the π and 3*d* spin states in the AFI ground state and the mechanism of phase transition from PM to AFI in this system. We observed, below T_{MI}, a characteristic shoulder in the magnetic susceptibility where the Schottky anomaly is observed in the specific heat. The *paramagnetic* 3*d* spin state surrounded by an AF-ordered π spin well reproduces the observable magnetic susceptibility and specific heat in the AFI ground state of λ-$BETS_2Fe_xGa_{1-x}Cl_4$. The 3*d* spin degrees of freedom in the AFI phase enable precise evaluation of the internal magnetic fields $H_{\pi d}$ induced by the π spin ordering, where $H_{\pi d}$ were proportional to the Fe content in λ-$BETS_2Fe_xGa_{1-x}Cl_4$ system. We concluded that Fe 3*d* spin provides favorable conditions for the PM-AFI transition in a strongly-correlated π electron system. Based on these results, we proposed a new mechanism of PM-AFI transition.

Acknowledgments

We thank H. Kobayashi, A. Kobayashi, B. Zhou, R. Kato and M. Ogata for valuable discussions and comments. This work was partially supported by a Grant-In-Aid for Scientific Research from the Ministry of Education, Culture, Sports, Science and Technology of Japan (Nos. 22-10866, 15340123, and 21110520), and Research Fellowships from the Japan Society for the Promotion of Science for Young Scientists.

References

1. Kobayashi, H.; Tomita, H.; Naito, T.; Kobayashi, A.; Sakai, F.; Watanabe, T.; Cassoux, P. New BETS conductors with magnetic anions. *J. Am. Chem. Soc.* **1996**, *118*, 368–377.
2. Akutsu, H.; Arai, E.; Kobayashi, H. Highly correlated organic conductor with magnetic anions exhibiting a π-*d* Coupled Metal-Insulator Transition, λ-$(BETS)_2FeBr_xCl_{4-x}$. *Am. Chem. Soc.* **1997**, *119*, 12681–12682.
3. Kobayashi, H.; Cui, H.; Kobayashi, A. Organic metals and superconductors based on BETS. *Chem. Rev.* **2004**, *104*, 5265–5288.
4. Uji, S.; Shinagawa, H.; Terashima, T.; Yakabe, T.; Terai, Y.; Tokumoto, M.; Kobayashi, A.; Tanaka, H.; Kobayashi, H. Magnetic-field-induced superconductivity in a two-dimensional organic conductor. *Nature* **2001**, *410*, 908–910.
5. Tokumoto, M.; Naito, T.; Kobayashi, H.; Kobayashi, A.; Laulhin, V.; Brossard, V.N.; Cassoux, L.P. Magnetic anisotropy of organic conductor λ-$(BETS)_2FeCl_4$. *Synth. Met.* **1997**, *86*, 2161–2162.
6. Brossard, L.; Clerac, R.; Coulon, C.; Tokumoto, M.; Ziman, T.; Petrov, D.K.; Laukin, V.N.; Naughton, M.J.; Audouard, A.; Goze, F.; *et al*. Interplay between chains of $S = 5/2$ localised spins and two-dimensional sheets of organic donors in the synthetically built magnetic multilayer λ-$(BETS)_2FeCl_4$. *Eur. Phys. J. B* **1998**, *1*, 439–452.
7. Kobayashi, A.; Udagawa, T.; Tomita, H.; Naito, T.; Kobayashi, H. New Organic Metals Based on BETS Compounds with $MX4^-$ Anions (BETS = bis(ethylenedithio)tetraselenafulvalene; M = Ga, Fe, In; X = Cl, Br). *Chem. Lett.* **1993**, *22*, 2179–2182.

8. Kobayashi, H.; Udagawa, T.; Tomita, H.; Bun, K.; Naito, T.; Kobayashi, A. A new organic superconductor, λ-(BEDT-TSF)$_2$GaCl$_4$. *Chem. Lett.* **1993**, 1559–1562.
9. Cui, H.; Kobayashi, H.; Kobayashi, A. Phase diagram and anomalous constant resistivity state of a magnetic organic superconducting alloy, λ-(BETS)$_2$Fe$_x$Ga$_{1-x}$Cl$_4$. *J. Mater. Chem.* **2007**, *17*, 45–48.
10. Negishi, E.; Uozaki, H.; Ishizaki, Y.; Tsuchiya, H.; Endo, S.; Abe, Y.; Matsui, H.; Toyota, N. Specific heat studies for λ-(BEDT-TSF)$_2$FeCl$_4$. *Synth. Met.* **2003**, *133–134*, 555–556.
11. Akiba, H.; Nakano, S.; Nishio, Y.; Kajita, K.; Zhou, B.; Kobayashi, A.; Kobayashi, H. Mysterious paramagnetic states of Fe 3*d* spin in antiferromagnetic insulator of λ-BETS$_2$FeCl$_4$ system. *J. Phys. Soc. Jpn.* **2009**, *78*, doi:10.1143/JPSJ.78.033601.
12. Ishizaki, Y.; Uozaki, H.; Tsuchiya, H.; Abe, Y.; Negishi, E.; Matsui, H.; Endo, S.; Toyota, N. Specific heat of organic superconductor λ-(BEDT-TSF)$_2$GaCl$_4$. *Synth. Met.* **2003**, *133*, 219–220.
13. Hiraki, K.; Mayaffre, H.; Horvatic, M.; Berthier, C.; Uji, S.; Yamaguchi, T.; Tanaka, H.; Kobayashi, A.; Kobayashi, H.; Takahashi, T. ^{77}Se NMR evidence for the Jaccarino-Peter mechanism in the field induced superconductor, λ-(BETS)2FeCl$_4$. *J. Phys. Soc. Jpn.* **2007**, *76*, doi:10.1143/ JPSJ.76.124708.
14. Mori, T.; Katsuhara, M. Estimation of πd-interactions in organic conductors including magnetic anions. *J. Phys. Soc. Jpn.* **2002**, *71*, 826–844.
15. Akiba, H.; Nobori, K.; Shimada, K.; Nishio, Y.; Kajita, K.; Zhou, B.; Kobayashi, A.; Kobayashi, H. Magnetic and thermal properties of λ-(BETS)$_2$FeCl$_4$ system—Fe 3*d* spin in antiferromagnetic insulating phase. *J. Phys. Soc. Jpn.* **2001**, *80*, doi:10.1143/JPSJ.80.063601.
16. Sasaki, T.; Uozaki, H.; Endo, S.; Toyota, N. Magnetic torque of λ-(BETS)$_2$FeCl$_4$. *Synth. Met.* **2001**, *120*, 759–760.
17. Waerenborgh, J.C.; Rabaca, S.; Almeida, M.; Lopes, E.B.; Kobayashi, A.; Zhou, B.; Brooks, J.S. Mössbauer spectroscopy and magnetic transition of λ-(BETS)$_2$FeCl$_4$. *Phys. Rev. B* **2009**, *81*, doi:10.1103/PhysRevB.81.060413.
18. Cepas, O.; McKenzie, R.H.; Merino, J. Magnetic-field-induced superconductivity in layered organic molecular crystals with localized magnetic moments. *Phys. Rev. B* **2002**, *65*, doi:10.1103/ PhysRevB.65.100502.
19. Otsuka, T; Kobayashi, A.; Miyamoto, Y.; Kiuchi, J.; Nakamura, S.; Wada, N.; Fujiwara, E.; Fujiwara, H.; Kobayashi, H. Organic antiferromagnetic metals exhibiting superconducting transitions κ-(BETS)$_2$FeX$_4$ (X = Cl, Br): Drastic effect of halogen substitution on the successive phase transitions. *J. Solid State Chem.* **2001**, *159*, 407–412.
20. Kobayashi, H.; Tanaka, H.; Ojima, E.; Fujiwara, H.; Nakazawa, Y.; Otsuka, T.; Kobayashi, A.; Tokumoto, M.; Cassoux, P. Antiferromagnetism and superconductivity of BETS conductors with Fe^{3+} ions. *Synth. Met.* **2001**, *120*, 663–664.
21. Sato, A.; Ojima, E.; Akutsu, H.; Nakazawa, Y.; Kobayashi, H. Magnetic properties of λ-BETS$_2$(Fe$_x$Ga$_{1-x}$)Cl$_4$ exhibiting a superconductor-to-insulator transition ($0.35 < x < 0.5$). *Phys. Rev. B* **2000**, *61*, 111–114.